Low to intermediate energy elastic electron scattering from dichloromethane (CH_2Cl_2)

B A Hlousek[1], M F Martin[1], M Zawadzki[1,2], M A Khakoo[1], L E Machado[3], R R Lucchese[4], V A S da Mata[5], I Iga[5], M-T Lee[5] and M G P Homem[5]

[1] Department of Physics, California State University, Fullerton, California 92834, USA.
[2] Atomic Physics Division, Department of Atomic, Molecular and Optical Physics, Faculty of Applied Physics and Mathematics, Gdańsk University of Technology, ul. G. Narutowicza 11/12, 80-233 Gdańsk, Poland.
[3] Departamento de Física, Universidade Federal de São Carlos, 13565-905 São Carlos, SP, Brazil
[4] Department of Chemistry, Texas A&M University, College Station, Texas 77842-3012, USA
[5] Departamento de Química, Universidade Federal de São Carlos, 13565-905 São Carlos, SP, Brazil

E-mail: `mghomem@ufscar.br; mkhakoo@fullerton.edu`

Abstract. We report a theoretical-experimental investigation of electron scattering by dichloromethane (CH_2Cl_2) in the low- and intermediate energy ranges. Experimental elastic differential cross sections (DCS), in the incident electron energy range of 0.5 to 800 eV and scattering angle range of 10^o to 130^o, were measured using a crossed beam relative flow technique. Integral and momentum-transfer cross sections were determined from the experimental DCS. Theoretical elastic differential, integral, and momentum-transfer, as well as grand-total, and total absorption cross sections were also calculated for impact energies ranging from 0.5 to 500 eV. A complex optical Hartree-Fock potential represented the electron-target interaction and a single-center expansion method combined with a Padé approximation was used to solve the scattering equations. Three resonances: a $^2A_1$ C-Cl kσ^* resonance centered at about 3.5 eV, a $^2B_2$ C-Cl kσ^* resonance centered at about 5 eV and a broad $^2A_1$ C-H kσ^* resonance at about 10 eV were detected in our calculation. Further calculations of DCS were performed at an intermediate energy range of 50 to 800 eV, using the independent-atom model in which the atomic complex optical potential and partial-wave method were used to obtain atomic scattering amplitudes. Comparisons of our experimental and theoretical data with very recent experimental and theoretical results are made.

Submitted to: *J. Phys. B: At. Mol. Phys.*

1. Introduction

Electron scattering from chlorine containing compounds has many important applications. It is significant in etching processes as source of chlorine atoms [1–3] and is also frequently used in organic chemistry as both reactants and solvents. As results of these applications, there is an expected increase in the concentration of chlorine containing molecules in the atmosphere, which has environmental consequences. Many such chlorine compounds have long atmospheric lifetimes and may stay in the Earth's troposphere for several decades [4]. In this condition, they interact with UV radiation, resulting in the formation of neutral and ionized molecules or radicals such as chlorine atoms which act as catalysts in chain reactions leading to the destruction of stratospheric ozone. On the other hand, a recent study has shown that even short-atmospheric-lifetime compounds such as CH_2Cl_2 have their concentrations increased in the atmosphere and consequently may be responsible for the loss of the ozone in the lower stratosphere [5].

The development of new technologies aiming to control the emission of such compounds into atmosphere is therefore of sufficient interest. Recently, non-thermal plasma processing (NPP) has been used as a modern and efficient technique to eliminate small concentrations of volatile organic compounds from industrial waste-gas streams [6]. Compared to more established technologies such as catalytic oxidation, thermal decomposition, etc., NPP is better-suited to remove chlorinated compounds especially those which are species particularly difficult to decompose [7, 8]. It is expected that the electron-collision cross sections of chlorine substituted methanes would be important to shed light on the underlying physics of such processes since they are necessary for the determination of the reactional rates [2, 3, 9]. In view of the needs of such collision data, a joint collaboration has been setup between electron collision groups located at Universidade Federal de São Carlos (UFSCar) and California State University Fullerton (CSUF) to obtain experimental and theoretical differential cross sections (DCS) on electron scattering for chlorinated hydrocarbons over wide incident electron energy (E) range. At the time this project started, except for chloromethane (CH_3Cl) [10–13] and carbon tetrachloride (CCl_4) [14, 15] there was a paucity of experimental and theoretical data of electron collisions with such molecules available in the literature, and CH_2Cl_2 was considered an excellent candidate to begin with.

For CH_2Cl_2, previous experimental studies include the total cross section (TCS) measurements of Karwasz *et al.* [13] in the E range of 75 to 4000 eV. There are also experimental and theoretical determinations of dissociative electron attachment cross sections by Aflatooni and Burrow [16, 17] and Gallup and Fabrikant [18], as well as rate coefficient measurements and product ion identification for thermal energy dissociative electron attachment reactions [19, 20].

On the theoretical side, DCS and momentum-transfer cross sections (MTCS) were reported by Natalense *et al.* [21, 22] in the 5 to 30 eV E range using the Schwinger multichannel method (SMC) with and without pseudo-potentials (SMCPP), the latter includes also polarization effects. Also, TCS, integral elastic cross sections (ICS) and total absorption cross sections (TACS) in the 20–5000 eV range were calculated by Naghma *et al* [23] using the spherical complex optical potential (SCOP) approach. Very recently, theoretical and experimental investigations on elastic electron scattering by CH_2Cl_2 were reported by Krupa *et al.* [24]. This work reports DCS calculated using two distinct theoretical models: the independent-atom with screen-correcting

additivity rule (IAM-SCAR) and the SMCPP. Experimental DCS at four incident energies and limited scattering angles (θ) were also reported. Their absolute value of DCS were obtained via normalization of the measured angular distributions to their theoretical results. At 7, 10, and 20 eV, the normalization was made to the SMCPP data at $\theta = 30^o$, and at 30 eV to IAM-SCAR data at same angle.

In the present work, experimental DCS for electron scattering by CH_2Cl_2 are reported in the extended 0.5 to 800 eV E range and for θ from 10^o to 130^o. The measurements at low E (0.5 to 30 eV) were performed at CSUF while those at the low to intermediate E (20 to 800 eV) were carried out in UFSCar. CSUF and UFSCar measurements at the overlapping E of 20 and 30 eV were made to check continuity of the measured DCS. Experimental ICS and MTCS were derived from the experimental DCS via numerical integration. Moreover, theoretical modeling of the electron–CH_2Cl_2 scattering was performed in UFSCar. The DCS, ICS, MTCS, TCS, and TACS were calculated using the molecular complex optical potential (MCOP) model combined with the Padé approximation in the 0.5 to 500 eV E range [25–31]. At 50 eV and above, DCS were also calculated using the standard independent-atom model (IAM), and ICS, MTCS and TCS were obtained in the additivity rule (AR) approach [32].

The organization of this paper is as follows: In section 2, we briefly describe experimental procedures used in both groups. In section 3, the theory and details of the UFSCar calculations are presented. In section 4, we present the experimental and theoretical results with comparisons between them and with other results available in the literature [13, 21, 22, 24]. In section 5, we summarize our work with some conclusions.

2. Experimental procedures

2.1. UFSCar Experiment

The UFSCar experimental apparatus has been well tested and is detailed in previous papers [31, 33]. The intensities of elastically scattered electrons from CH_2Cl_2 were measured using a crossed geometry of a collimated electron beam and a collimated molecular beam from a tube source. An unselected electron gun produced a stable electron beam in the E range of 20 eV to 1000 eV with typical electron currents ranging around 50-150 nA with an energy resolution of about 0.5 eV full-width at half-maximum. The scattered electrons were energy-filtered by a retarding-field analyzer which enabled the detection of elastically scattered electrons that were discriminated from inelastic scattered electrons (within an energy window of about 1.5 eV), by a retarding grid placed in front of the electron detecting channel multiplier. The analyzer is consequently able to separate elastically scattered electrons from those provided by electronic excitations, but not those scattered by vibrational inelastic scattering with energy loss < 1.5 eV. Therefore, the reported results of the UFSCar experiment are the summation of both vibrational elastic and inelastic cross sections. Three perpendicularly pairs of Helmholtz coils around the vacuum chamber reduced the magnetic fields to < 15mG. Details of our target gas sample handling system have also described previously [34]. The gas beam is collimated by a thin molybdenum tube with internal diameter of 1 mm and a diameter to length aspect ratio of 0.03. The liquid CH_2Cl_2 was purchased from Sigma-Aldrich with $\geq 99.8\%$ purity. The gaseous CH_2Cl_2 was obtained from the saturated vapor above a liquid sample in a

small vial attached to the gas handling system. Several cycles of freeze-pump-thaw degassing were performed in order to eliminate atmospheric air and other volatile dissolved contaminants. The purity of the gaseous CH_2Cl_2 was checked during the measurements using a quadrupole mass analyzer attached to the experimental chamber for contaminants emanating from the target and contaminations were found to be negligible.

The angular distributions of the scattered electrons were converted to absolute DCS using the relative flow technique (RFT) [35]. Argon and nitrogen were used as reference gases. Therefore, the elastic DCS for the target molecule can be related to those of the reference gas:

$$(DCS)_x = (DCS)_{std} \frac{I_x}{I_{std}} \frac{n_{std}}{n_x} \left(\frac{M_{std}}{M_x} \right)^{\frac{1}{2}}, \tag{1}$$

Where subscript x refers to the target molecule, *std* the standard (reference) gas, I is the electron scattering rate, n is the relative flow rate and M is the molecular weight. In general, at low target backing pressures where the mean-free path of the gas is comparable or fractionally less than the tube length, the flow rate can be written, to a good approximation, as a second order polynomial in P, the gas target backing pressure [34]: $n = k_1 P + k_2 P^2$. However, in this work, the normalization procedure was performed in a low-pressure regime ($P < 0.3$ Torr), where the mean-free path for collisions between the target molecules was comparable or greater than the collimating gas tube length, and the P^2 contribution was made negligible. Therefore, the formula for the RFT was reduced to:

$$(DCS)_x = (DCS)_{std} \frac{I_x}{I_{std}} \frac{P_{std}}{P_x}. \tag{2}$$

At E values of 20 and 30 eV, the experimental elastic DCS of molecular nitrogen reported by Shyn and Carignan [36] were used as a standard to normalize our data. At higher energies, argon was used as reference. For argon, the absolute DCS of Dubois and Rudd [37] at 50 and 800 eV and the DCS reported by Jansen *et al.* [38] in the 100 eV to 500 eV range were used. For each E, the angular distribution of the scattered electrons was measured at least 5 times to verify its reproducibility and the RFT normalization procedure was applied at least twice at several normalization angles. With the uncertainties reported for the reference gases and the uncertainties associated with the experimental procedure, the estimated standard deviations in the present DCS are 17% at 20 eV, 30 eV and 800 eV, 21% at 50 eV, and 11% at other energies.

2.2. CSUF Experiment

The CSUF experimental setup is detailed in e.g. Khakoo *et al.* [39]. We have used a well-tested electron spectrometer in which the electron gun and detector employed double hemispherical energy selectors made of titanium. Cylindrical lenses were used to transport scattered electrons through the system which was baked to about 80 to 130^{o}C with magnetically-free biaxial heaters [40] to maintain stability of the of surfaces in the experiment. Electrons were detected by a discrete dynode electron multiplier [41] with a dark count rate of < 0.01Hz and capable of linearly detecting $> 10^5$ Hz without saturating. The remnant magnetic field was reduced to ≈ 1 mG at the collision region by a double mu-metal shield. Typical electron currents were

around 18-25 nA, with an energy resolution of between 50-70 meV, full-width at half-maximum. Lower currents were chosen for lower E values to minimize space charge broadening of the incident electron beam. The electron beam could be focused at 0.5 eV and remained stable, varying less than 15% at maximum during the data acquisition period. The energy of the beam was established by measuring the minimum in the elastic scattering of the 2^2S He-resonance at 19.366 eV [42] at the θ of 90^o to $\approx$ 40 meV stability during a daily run. Typically the contact potential varied between 0.55 eV to 0.65 eV. The elastic peaks of the energy loss spectra were collected at fixed E and θ values by repetitive multi-channel-scaling techniques. The effusive target gas beam was formed by flowing gas through a 0.3 mm diameter aperture, which was sooted (using an acetylene flame) to reduce secondary electrons. In using the aperture source instead of a conventional tube gas collimator, we obviated the experimental need to maintain the backing pressures of the target gases in an inverse ratio of their molecular diameters (in order to equalize the mean free path of the two target gases [43] in the gas collimating structure) thus removing an additional systematic source of error that could occur in using tube collimator or similar setups, see e.g. [43]. This is a great advantage when working with heavy molecular targets of masses around 100 a.m.u. since the uncertainty in the molecular diameters of such targets can be considerable and applying the inverse molecular diameter gas pressure ratio accurately in the RFT at moderate or high target source pressures, is made more challenging with controlling the stability in the flow of these viscous mass targets through collimating needle sources. The aperture, located $\approx$ 7 mm below the axis of the electron beam, was incorporated into a movable source [43, 44] arrangement. The moveable gas source method determines background electron-gas scattering rates expediently and accurately [43]. The measured DCS were normalized using the RFT with helium as the reference gas, using DCS from the well-established work of Nesbet [45] for E $<$ 20 eV and of Register *et al.* [46] for E $\geq$ 20 eV. The pressures behind the aperture ranged from 1.2 to 1.8 Torr for He and 0.06 to 0.13 Torr for CH_2Cl_2, resulting in a chamber pressure ranging from 8×10^{-7} Torr to 1.8×10^{-6} Torr. The CH_2Cl_2 liquid was obtained from Sigma-Aldrich and was $\geq$ 99.8% purity. The liquid was placed in a 50 c.c. all glass-metal flask attached by baked 1/4-inch refrigeration copper tubing to the experimental gas handling system and the liquid sample was purified from dissolved gases in it by liquid N_2 freeze-pump cycles. CH_2Cl_2 has a large molecular mass (84.93 a.m.u.), but it is not the heaviest target used in our system. Its raised viscosity caused instabilities in the flow as our gas metering valve (Granville-Phillips Series 203 valve [47]) and therefore this valve was baked at a temperature of about $\approx 70^o$C. Also, the entire gas line after the metering valves was heated to $\approx 95^o$C to prevent condensation of CH_2Cl_2 in the valve and gas lines. Each DCS was taken a minimum of two times to check its reproducibility and weighted averaging was made of multiple data sets to obtain the final DCS.

The experimental ICS and MTCS were obtained by numerical integration of the final DCS. The DCS in the angular regions not covered by the experiment were obtained by extrapolation following the procedure previously described [48, 49]. An added error of about 20% is estimated in the integrated data to the average DCS errors when integrating to obtain ICS and MTCS because of the problem in extrapolating to small θ due to the small angle dipole-peaking of the elastic scattering DCS. The additional error is added in quadrature to the average error of the experimental DCS [49].

3. Theory and numerical procedure

The theory used in this work has been described previously [25–27, 31]. A complex potential composed of static-exchange, correlation-polarization, and absorption contributions is used to represent the interaction of electron and target. The static-exchange potential was derived from a near-Hartree-Fock self-consistent-field (HF-SCF) wave function of the target, whereas the correlation-polarization potential was obtained in the framework of the free-electron-gas model, derived from a parameter-free local density approach [50]. The absorption contribution was taken into account via the scaled quasi-free scattering model of Lee *et al.* [51] which is an improvement of the third version of the model absorption potential originally proposed by Staszewska *et al.* [52]. Using this potential, the electron scattering equation is solved iteratively using the [N/N] Padé approximation according to the method described previously in [53, 54].

The HF-SCF wave function of CH_2Cl_2 was obtained using the triple-zeta valence (TZV-3d) basis set of the Firefly QC package [55], which is partially based on the GAMESS (US) [56] source code. The point group C_{2v} was used in our calculations to describe the symmetry of the molecule. For the experimental ground state molecular geometry [57], this basis provided a total energy of -958.0573 hartrees. The calculated electric dipole moment was 1.83 D, about 14% larger than the experimental value of 1.60 D [57]. The asymptotic form of the correlation-polarization potential was generated using the presently calculated dipole polarizabilities α_{xx} = 33.27 a.u., α_{yy} =51.77 a.u. and α_{zz} = 33.22 a.u. Our value for α_0 = 39.42 a.u., is in good agreement with that of 40.79 a.u. [57] calculated at the HF-SCF level using the aug-cc-pVTZ basis set.

In our calculation, the target wave function and interaction potentials were partial-wave expanded about the center-of-mass of the molecule in terms of symmetry-adapted functions [58]. The truncation parameters used in these expansions were l_c = 40 for the bound orbitals and l_c = 80 for the interaction potentials. The cutoff parameter l_c = 30 was used for the continuum orbitals and for the T-matrix elements at 100 eV and above. At lower energies, l_c = 20 was used. The calculated cross sections generally converged after $\approx$ 10 iterations. Also, a rotating point-dipole Born-closure formula was used to take account of the effects of high partial-wave contributions to the scattering amplitudes. This procedure was similar to that used in some of our past works [25, 26]. For 50 eV and above, DCS were also calculated in the IAM framework. Details of the procedure and interaction potentials are given in our previous work [33]. Moreover, the ICS, MTCS and TCS were generated using the IAM-AR [32].

4. Results and discussion

The experimental DCS, ICS, and MTCS for elastic electron scattering by CH_2Cl_2 obtained in CSUF and UFSCar are listed in Tables 1 and 2, respectively. A comparison of the experimental DCS with our theoretical results, calculated at MCOP and IAM levels of approximation, and with the calculated and measured data of Krupa *et al.* [24] is shown in Figs. 1-3. In the 5 to 30 eV E range, the theoretical results of Natalense *et al.* [21, 22] using the SMC approach without including polarization effects are also shown. In Fig. 1, our measured data of CSUF group at 1, 3, 5, and 10 eV are compared with the present calculated results using the MCOP approach. At energies up to 5 eV, some unphysical oscillations appeared in the calculated MCOP DCS which were

caused by the poor convergence of the scattering wave functions due to the slow fall-off of the long-range potentials of dipole and quadrupole natures. The Born-closure procedure based on the rotating point-dipole model [19] was unable to eliminate such oscillations. Therefore, the MCOP DCS at 1, 3, and 5 eV presented in these figures were submitted to a smoothing procedure. Overall, we find a fairly good agreement between the experimental DCS and the MCOP data at angles up to 90^o. At 5 eV, the SMC data of Natalense *et al.* [21, 22] also agree well with our data. At 10 eV, our experimental DCS show very good agreement with both the present MCOP results and the SMCPP data of Krupa *et al.* [24]. Particularly, a shoulder at near 25^o and a shallow minimum at near 110^o seen in our experimental data are reproduced by both calculations. The calculated SMC results of Natalense *et al.* [21, 22] also agree reasonably with our theoretical and experimental data except at near-forward direction where their calculated data are unable to describe the forward peaking behavior of DCS, due to the absence of both permanent and induced dipole effects in their theory. On the other hand, the calculated DCS using the IAM-SCAR method of Krupa *et al.* [24] did not present the shoulder at near 25^o and also show a pronounced minimum near 115^o that is not observed by the experiments. This is not surprising since this model is not expected to work well at low E values. The experimental DCS of Krupa *et al.* [24] at small θ are significantly higher than our experimental and also all the theoretical results by a factor greater than 2. Particularly, their results present a much steeper forward-peaking behavior than our data. At $\theta \geq 30^o$, only four experimental data were reported by Krupa *et al.*. Despite that, their DCS and ours from the CSUF show very good agreement.

In Fig. 2, the experimental DCS obtained by both the CSUF and the UFSCar groups at E = 20 and 30 eV are compared with the MCOP results, the calculated and measured data of Krupa *et al.* [24], and with the SMC results of Natalense *et al.* [21, 22]. It is seen that there is a very good agreement between the CSUF and UFSCar data. Since those results were obtained using different experimental setups as well as different normalization procedures, the observed good agreement seems to reinforce the accuracy of both data sets. Their comparison with the theories shows that the MCOP calculations are able to reproduce the structures seen in the experimental data. Especially, the shoulder at near 45^o, a minimum at about 70^o and a maximum at about 110^o are very well reproduced. Quantitatively, the agreement between the MCOP and experimental results is also very good for θ up to 70^o. There is also a generally good agreement between the SMCPP data [24] and our experimental results, particularly at scattering angles up to 50^o. On the other hand, although the SMC DCS [21, 22] agree well with our experimental data at E = 20 eV, they are in significant disagreement at E = 30 eV. As expected, the reliability of the IAM-SCAR calculations improves with increasing incident energies. For instance at 30 eV, the IAM-SCAR calculations were able to reproduce quite well the minima at around 70^o and 140^o of our MCOP data. However, these minima are not easily seen in the experimental data of Krupa *et al.* [24] due to the angular sparseness of their measurement, particularly above 50^o. Comparison of their data at 20 eV with the present measured DCS shows agreement at some angles and discrepancy at others. Specifically, at 10^o, their DCS is found to be almost a factor of 2 lower than ours. However, their data at this energy present an extremely steep forward-peaking behavior even compared to their results at 10 and 30 eV, in the sense that the DCS at 8^o could not included in Fig. 2. At E = 30 eV, the experimental DCS of Krupa *et al.* are found to be higher than the present experimental DCS by about a factor of 2 except at $\theta = 60^o$, 70^o and 120^o where they

agree to our measured data within the experimental uncertainties.

In Fig. 3 we compare the experimental results at energies ranging from 50 to 500 eV, obtained by the UFSCar group, with our MCOP data. Here the theoretical results obtained using the standard IAM approach are also presented. At 50 and 100 eV, there is an excellent agreement both qualitatively and quantitatively between the MCOP theory and experiments. At these energies, the IAM calculations were also able to reproduce the minima at about 70^o and 120^o, but not the shoulder at near $30^o$of the experimental data. At 200 eV, the MCOP results agree well with the measured data except the deep minimum seen at around 100^o in the experimental DCS, which appears too shallow in the MCOP calculations. At 500 eV, there is a generally good agreement between our MCOP results and experimental data. However, small oscillations are shown in the calculated DCS which are due to the lack of convergence in the partial-wave expansion of the scattering wave functions [31]. On the other hand, there is a very good agreement between the experiments and IAM calculations at that energy in the entire scattering angular range.

In Fig. 4, we show the fixed-angle elastic scattering DCS taken at 90^o as a function of E with closely spaced intervals of 0.0524 eV and normalized to the DCS ($\theta = 90^o$) listed in Table 1 at 4 eV. Comparison of these data were made with the theoretical fixed-angle DCS calculated using the MCOP approach. It is seen that the theoretical curve exhibits 3 features: a bump at near 3 eV, a peak at near 5 eV, and a broad enhancement at near 8 eV. Such features suggest the occurrence of shape resonances. Our experimental data also exhibit clearly a broad resonance-like feature at E about 8 eV. A weak shoulder at about E = 3.5 eV is also barely discerned. Moreover, the θ = 90^o DCS rise steeply as E $\rightarrow$ 0 eV, indicating the role of polar nature of the target. This behavior is also reproduced by the MCOP calculations. In general, there is a good agreement between the calculated and experimental fixed-angle DCS at energies below 12 eV. The theory overestimates the experimental data at higher energies.

In Fig. 5, the present experimental ICS and MTCS are compared with the experimental ICS of Krupa *et al.* [24] and with our theoretical ICS and MTCS calculated using both the MCOP and IAM-AR. The ICS calculated using the SMCPP with Born closure and the IAM-SCAR model of Krupa *et al.* [24], the SCOP ICS of Naghma *et al.* [23], and the SMC MTCS of Natalense *et al.* [21] are also shown for comparison. Our calculated ICS and MTCS using the MCOP present a small peak at E about 5 eV and a broad enhancement at around 10 eV. Corresponding features were also seen in our calculated fixed-angle DCS located at about 5 and 8 eV, shown in Fig. 4. The bump at near 3.5 eV seen in Fig. 4 is also barely confirmed here. In order to better understand the physical origin of these structures, a partial-channel ICS analysis (using ICS without Born correction) was made and is shown in Fig. 6. From this analysis, it is seen that the peak near 5 eV is in fact due to a sharp $^2B_2$ C-Cl kσ^* resonance whereas the broad enhancement at about 10 eV is originated by the sum of $^2A_1$ (at 10 eV), the $^2B_1$ (at 7.5 eV), and the $^2A_2$ (at 15 eV) resonances. The enhancement at about 10 eV is also seen in the experimental data, whereas the peak located at near 5 eV cannot be clearly identified. Moreover, the partial cross-section analysis has also revealed that there is in fact a broad resonance at near 3.5 eV which is attributed to the $^2A_1$ C-Cl kσ^* shape resonance and seems to support the feature in the MCOP fixed-angle DCS and also the barely discerned structure in the experimental $\theta = 90^o$ DCS seen in Fig. 4 at about the same E. However, this resonance became very weak in our theoretical ICS and MTCS curves when the partial cross sections were added up. The calculated ICS of Krupa *et al.*[24] using the SMCPP

plus Born correction have revealed three resonance features located at 0.5 eV (A_1), 2.3 eV (B_2), and 10 eV (A_1+A_2+B_1), respectively. The fact that the first two resonances of their work are shifted to lower energies relative to ours is due to the different ways to account for the polarization effects in the calculations. The dependence of the position and width of resonances on the polarization potential is clearly shown in Fig. 3 in their work and was also discussed in some of our previous works [29, 31]. Quantitatively, the present experimental ICS data agree very well with our calculated results using both the MCOP and IAM-AR, and with the SMCPP+Born ICS of Krupa *et al.* [24] while the IAM-SCAR calculations [24] overestimate systematically our experimental data. On the other hand, the SCOP ICS of Naghma *et al.* are about 30% lower than our MCOP data for E > 30 eV, still they agree marginally with our experimental ICS. Regarding the experimental ICS of Krupa *et al.* [24], we note that despite the significant discrepancy seen between their and our experimental DCS, their results agree to ours within the error bars. For MTCS, our MCOP calculations reproduce reasonably well the present experimental results. The SMC MTCS of Natalense *et al.* [21] and present IAM MTCS also agree well with our data.

For the sake of completeness, in Figs. 7(a) and 7(b) we present our MCOP TCS and TACS, respectively, for electron scattering by CH_2Cl_2 in the 1–500 eV range. In Fig. 7(a), we compare our MCOP TCS with the experimental TCS reported by Karwasz *et al.* [13]. The calculated TCS of Krupa *et al.* using the IAM-SCAR model, the SCOP TCS of Naghma *et al.*, and the present IAM-AR TCS are also shown for comparison. It is seen that the MCOP TCS agrees very well with the experimental results of Karwasz *et al.* [13] especially for E > 100 eV. At these energies, the TCS calculated using the IAM-SCAR, IAM-AR, and SCOP also agree reasonably well with our data. Nevertheless, the IAM-SCAR significantly overestimate our calculation at lower energies. In Fig. 7(b), the calculated TACS using the MCOP are compared with the SCOP TACS of Naghma *et al.* [23] and the IAM-SCAR TACS of Krupa *et al.* [24]. It is seen that both SCOP TACS and IAM-SCAR TACS lie systematically higher than our data.

5. Summary

This study reports a joint theoretical-experimental investigation on electron collision with CH_2Cl_2 over a wide E range. Experimental DCS, ICS, and MTCS are reported in the E = 0.5 eV to 800 eV range. Theoretical DCS, ICS, MTCS, TCS, and TACS up to 500 eV are calculated using a combination of MCOP and Padé approximation and with the standard IAM approach. Experimentally, measurements at low E (up to 30 eV) were carried out in CSUF and in the 20–800 eV performed in UFSCar. The reliability of our experimental data is supported by the good agreement between the measured DCS of CSUF and UFSCar at overlaping E = 20 eV and 30 eV, using different experimental setups and procedures. Such reliability is also supported by the present theoretical investigation using a combination of MCOP and Padé approximation methods, the SMCPP calculation of Krupa *et al.* [24], and by the present IAM calculations. Finally, we expect that the present experimental DCS, measured covering wide ranges of E and θ, could be very useful for the further theoretical developments and also experimental studies of this target. Our investigation may also contribute to the efforts to provide collision data for modeling to understand underlying physics in various technological applications mentioned in the introductory section.

Acknowledgments

This research was supported by the Brazilian agencies FAPESP (grant no. 2015/08258-2), CNPq (grant no. 311152/2016-3), CAPES, and also by the US National Science Foundation (grants no. NSF-RUI-AMO 1306742 and 0968874). M. Zawadzki was funded by a Fulbright Fellowship.

References

[1] Donnelly V M and Kornblit A 2013 *Journal of Vacuum Science & Technology A: Vacuum, Surfaces, and Films* **31** 050825
[2] Kemaneci E, Carbone E, Booth J P, Graef W, van Dijk J and Kroesen G 2014 *Plasma Sources Science and Technology* **23** 045002
[3] Huang S and Gudmundsson J T 2014 *Plasma Sources Science and Technology* **24** 015003
[4] Wallington T J, Hurley M D and Schneider W F 1996 *Chemical Physics Letters* **251** 164–173
[5] Hossaini R, Chipperfield M P, Montzka S A, Leeson A A, Dhomse S S and Pyle J A 2017 *Nature Communications* **8** 15962
[6] Fitzsimmons C, Ismail F, Whitehead J C and Wilman J J 2000 *The Journal of Physical Chemistry A* **104** 6032–6038
[7] Abd Allah Z, Whitehead J C and Martin P 2014 *Environmental Science & Technology* **48** 558–565
[8] Zhu R, Mao Y, Jiang L and Chen J 2015 *Chemical Engineering Journal* **279** 463–471
[9] Bartschat K and Kushner M J 2016 *Proceedings of the National Academy of Sciences* **113** 7026–7034
[10] Shi X, Chan V K, Gallup G A and Burrow P D 1996 *The Journal of Chemical Physics* **104** 1855–1863
[11] Kato H, Asahina T, Masui H, Hoshino M, Tanaka H, Cho H, Ingólfsson O, Blanco F, Garcia G, Buckman S J and Brunger M J 2010 *The Journal of Chemical Physics* **132** 074309
[12] Navarro C, Sakaamini A, Cross J, Hargreaves L R, Khakoo M A, Fedus K, Winstead C and McKoy V 2015 *Journal of Physics B: Atomic, Molecular and Optical Physics* **48** 195202
[13] Karwasz G P, Brusa R S, Piazza A and Zecca A 1999 *Physical Review A* **59** 1341
[14] Limão Vieira P, Horie M, Kato H, Hoshino M, Blanco F, García G, Buckman S J and Tanaka H 2011 *The Journal of Chemical Physics* **135** 234309
[15] Zecca A, Karwasz G P and Brusa R S 1992 *Phys. Rev. A* **46** 3877–3882
[16] Aflatooni K, Gallup G A and Burrow P D 2000 *The Journal of Physical Chemistry A* **104** 7359–7369
[17] Aflatooni K and Burrow P D 2001 *International Journal of Mass Spectrometry* **205** 149–161
[18] Gallup G A and Fabrikant I I 2011 *The Journal of Chemical Physics* **135** 134316
[19] Miller T M, Friedman J F, Schaffer L C and Viggiano A A 2009 *The Journal of Chemical Physics* **131** 084302
[20] Burns S J, Matthews J M and McFadden D L 1996 *The Journal of Physical Chemistry* **100** 19436–19440
[21] Natalense A P P, Bettega M H F, Ferreira L G and Lima M A P 1999 *Physical Review A* **59** 879
[22] Natalense A P P, Varella M T d N, Bettega M H F, Ferreira L G and Lima M A P 2001 *Brazilian Journal of Physics* **31** 15–20
[23] Naghma R, Gupta D and Antony B 2014 *Journal of Electron Spectroscopy and Related Phenomena* **193** 48 – 53
[24] Krupa K, Lange E, Blanco F, Barbosa A S, Pastega D F, Sanchez S d, Bettega M H F, García G, Limão Vieira P and da Silva F F 2018 *Physical Review A* **97** 042702
[25] Rawat P, Homem M G P, Sugohara R T, Sanches I P, Iga I, de Souza G L C, dos Santos A S, Lucchese R R, Machado L E, Brescansin L M and Lee M T 2010 *Journal of Physics B: Atomic, Molecular and Optical Physics* **43** 225202
[26] de Souza G L C, Lee M T, Sanches I P, Rawat P, Iga I, dos Santos A S, Machado L E, Sugohara R T, Brescansin L M, Homem M G P and Lucchese R R 2010 *Physical Review A* **82** 012709
[27] Lee M T, de Souza G L C, Machado L E, Brescansin L M, dos Santos A S, Lucchese R R, Sugohara R T, Homem M G P, Sanches I P and Iga I 2012 *The Journal of Chemical Physics* **136** 114311

[28] Homem M G P, Iga I, Ferraz J R, dos Santos A S, Machado L E, de Souza G L C, Brescansin L M, Lucchese R R and Lee M T 2015 *Physical Review A* **91** 012713
[29] Homem M G P, Iga I, da Silva L A, Ferraz J R, Machado L E, de Souza G L C, da Mata V A S, Brescansin L M, Lucchese R R and Lee M T 2015 *Physical Review A* **92** 032711
[30] de Souza G L C, da Silva L A, de Sousa W J C, Sugohara R T, Iga I, dos Santos A S, Machado L E, Homem M G P, Brescansin L M, Lucchese R R and M-T L 2016 *Physical Review A* **93** 032711
[31] da Silva L A, da Mata V A S, de Souza G L C, Iga I, Machado L E, Lucchese R R, Lee M T and Homem M G P 2016 *Physical Review A* **94** 052704
[32] Raj D 1991 *Physics Letters A* **160** 571–574
[33] Homem M G P, Sugohara R T, Sanches I P, Lee M T and Iga I 2009 *Physical Review A* **80** 032705
[34] Homem M G P, Iga I, Sugohara R T, Sanches I P and Lee M T 2011 *Review of Scientific Instruments* **82** 013109
[35] Srivastava S K, Chutjian A and Trajmar S 1975 *The Journal of Chemical Physics* **63** 2659–2665
[36] Shyn T W and Carignan G R 1980 *Physical Review A* **22** 923
[37] DuBois R D and Rudd M E 1976 *Journal of Physics B: Atomic and Molecular Physics* **9** 2657
[38] Jansen R H J, de Heer F J, Luyken H J, van Wingerden B and Blaauw H J 1976 *Journal of Physics B: Atomic and Molecular Physics* **9** 185
[39] Khakoo M A, Beckmann C E, Trajmar S and Csanak G 1994 *Journal of Physics B: Atomic, Molecular and Optical Physics* **27** 3159
[40] Ari industries inc., addison, il 60101 usa, 1hn040b-16.3 biaxial cable
[41] Etp equipe thermodynamique et plasmas (etp) model af151
[42] Brunt J N H, King G C and Read F H 1977 *Journal of Physics B: Atomic and Molecular Physics* **10** 433
[43] Khakoo M A, Keane K, Campbell C, Guzman N and Hazlett K 2007 *Journal of Physics B: Atomic, Molecular and Optical Physics* **40** 3601
[44] Hughes M, James Jr K E, Childers J G and Khakoo M A 2003 *Measurement Science and Technology* **14** 841
[45] Nesbet R K 1979 *Physical Review A* **20** 58
[46] Register D F, Trajmar S and Srivastava S K 1980 *Physical Review A* **21** 1134
[47] Mks, granville-phillips division, 6450 dry creek parkway, longmont, co 80503 usa
[48] Buk M V, Bardela F P, Silva L A, Iga I and Homem M G P 2018 *Journal of Physics B: Atomic, Molecular and Optical Physics* **51** 095201
[49] Fedus K, Navarro C, Hargreaves L R, Khakoo M A, Silva F M, Bettega M H F, Winstead C and McKoy V 2014 *Phys. Rev. A* **90** 032708
[50] Perdew J P and Zunger A 1981 *Phys. Rev. B* **23**(10) 5048–5079
[51] Lee M T, Iga I, Machado L E, Brescansin L M, y Castro E A, Sanches I P and de Souza G L C 2007 *Journal of Electron Spectroscopy and Related Phenomena* **155** 14–20
[52] Staszewska G, Schwenke D W and Truhlar D G 1984 *Physical Review A* **29** 3078
[53] Gianturco F A, Lucchese R R and Sanna N 1994 *The Journal of Chemical Physics* **100** 6464–6471
[54] Natalense A P P and Lucchese R R 1999 *The Journal of Chemical Physics* **111** 5344–5348
[55] Granovsky A A Firefly version 8, http://classic.chem.msu.su/gran/firefly/index.html
[56] Schmidt M W, Baldridge K K, Boatz J A, Elbert S T, Gordon M S, Jensen J H, Koseki S, Matsunaga N, Nguyen K A, Su S, Windus T L, Dupius M and Montgomery J A 1993 *Journal of Computational Chemistry* **14** 1347–1363
[57] Nist computational chemistry comparison and benchmark database release 18, October 2016 URL `http://cccbdb.nist.gov/`
[58] Burke P G, Chandra N and Gianturco F A 1972 *Journal of Physics B: Atomic and Molecular Physics* **5** 2212

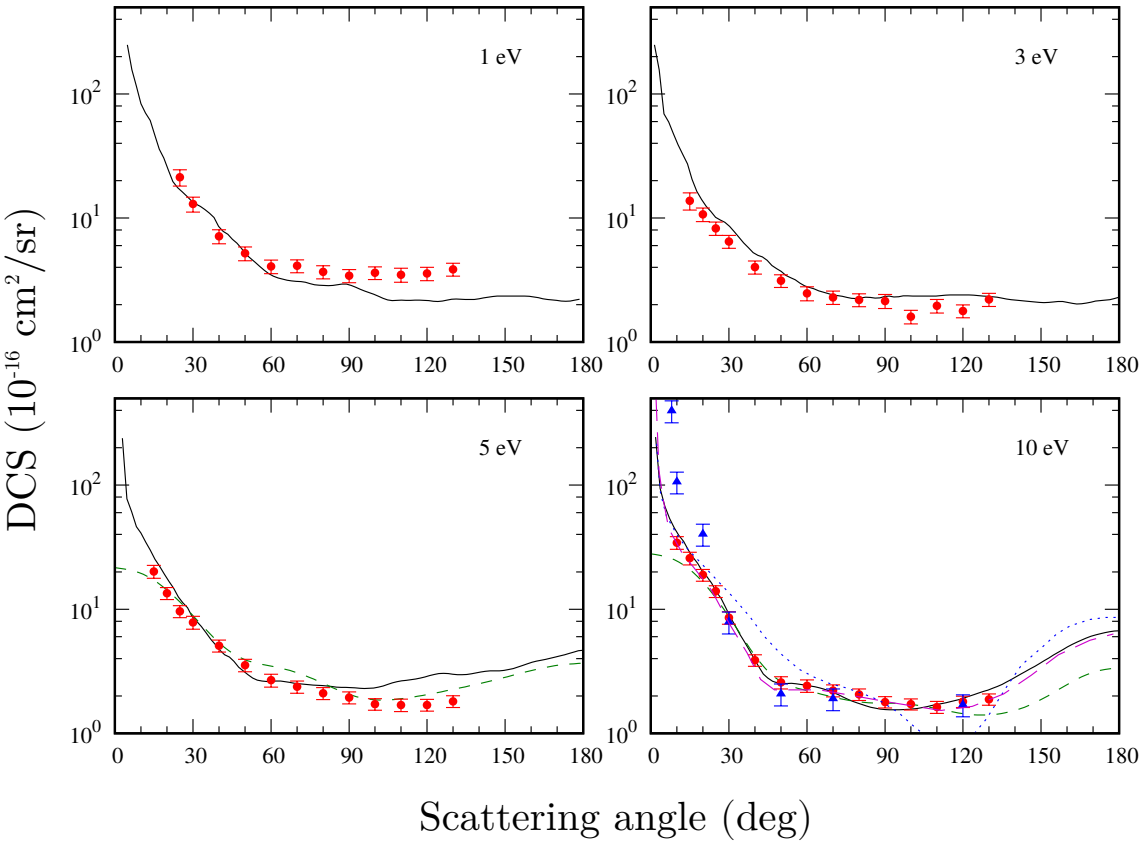

Figure 1. (color online) DCS for elastic scattering from CH_2Cl_2 at E = 1 eV, 3 eV, 5 eV and 10 eV. Experiment: (●) Present CSUF data; (▲) Krupa *et al.* [24]. Theory: (——) Present MCOP results; (- - -) SMC results from Natalense *et al.* [21, 22]; (·····) IAM-SCAR and (– – –) SMCPP from [24].

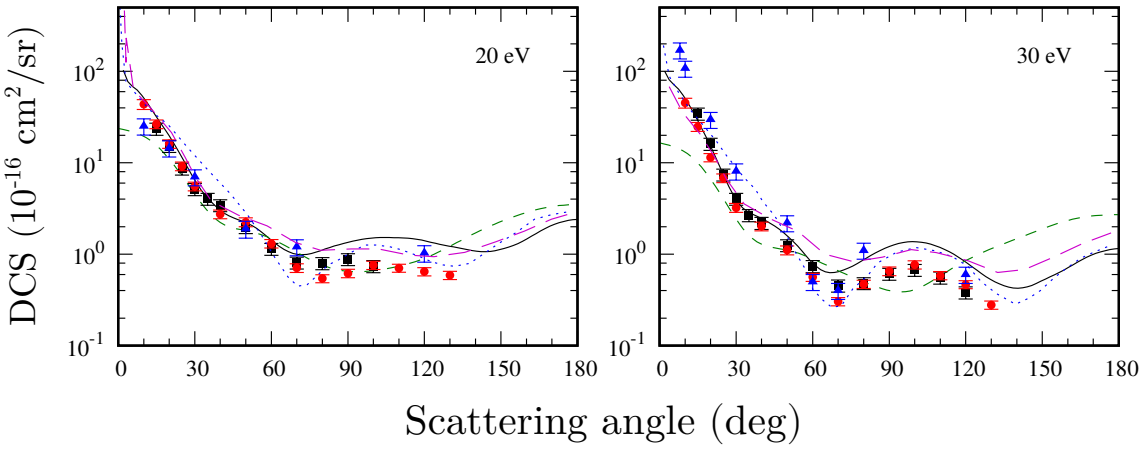

Figure 2. (color online) DCS for elastic scattering from CH_2Cl_2 at E = 20 eV and 30 eV, where the UFSCar and CSUF data sets overlap in E. Same as Fig. 1, except (■) present UFSCar data.

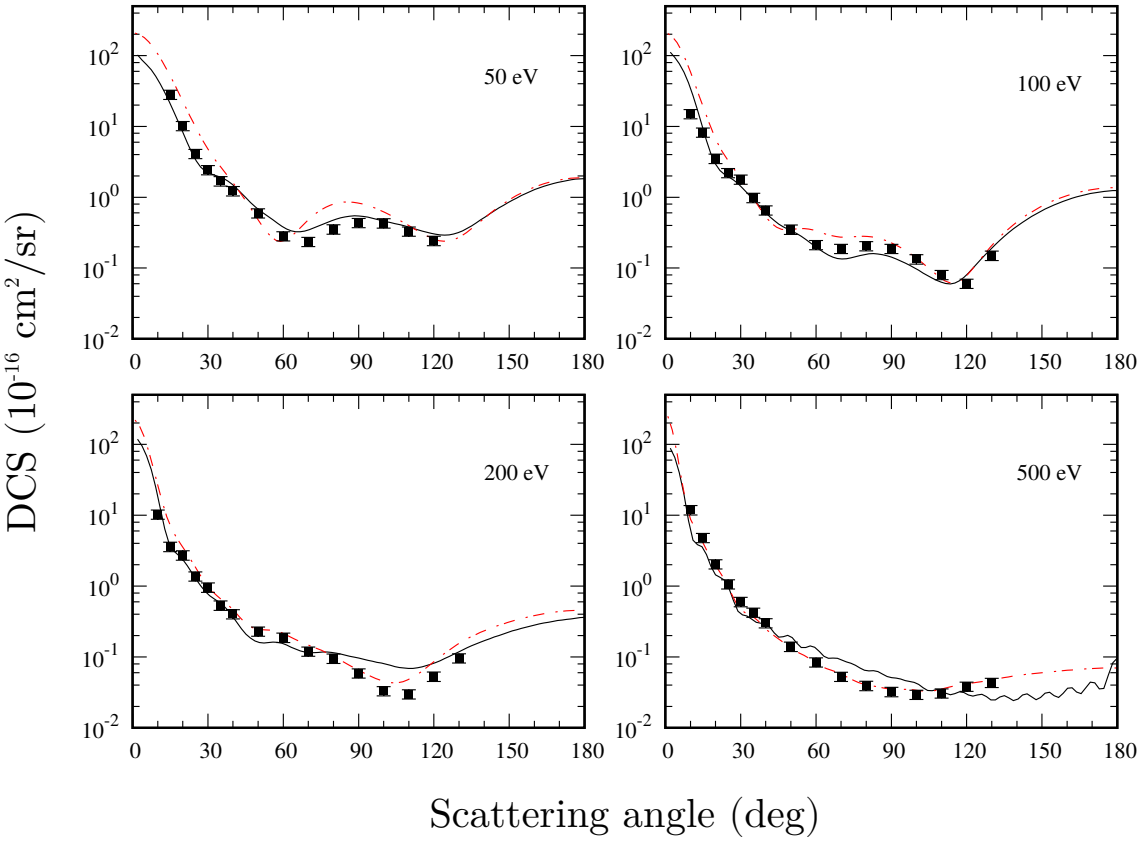

Figure 3. (color online) DCS for elastic scattering from CH_2Cl_2 at E = 50 eV, 100 eV, 200 eV and 500 eV. Same as Fig. 1 and 2, except (-·-·-) present IAM results.

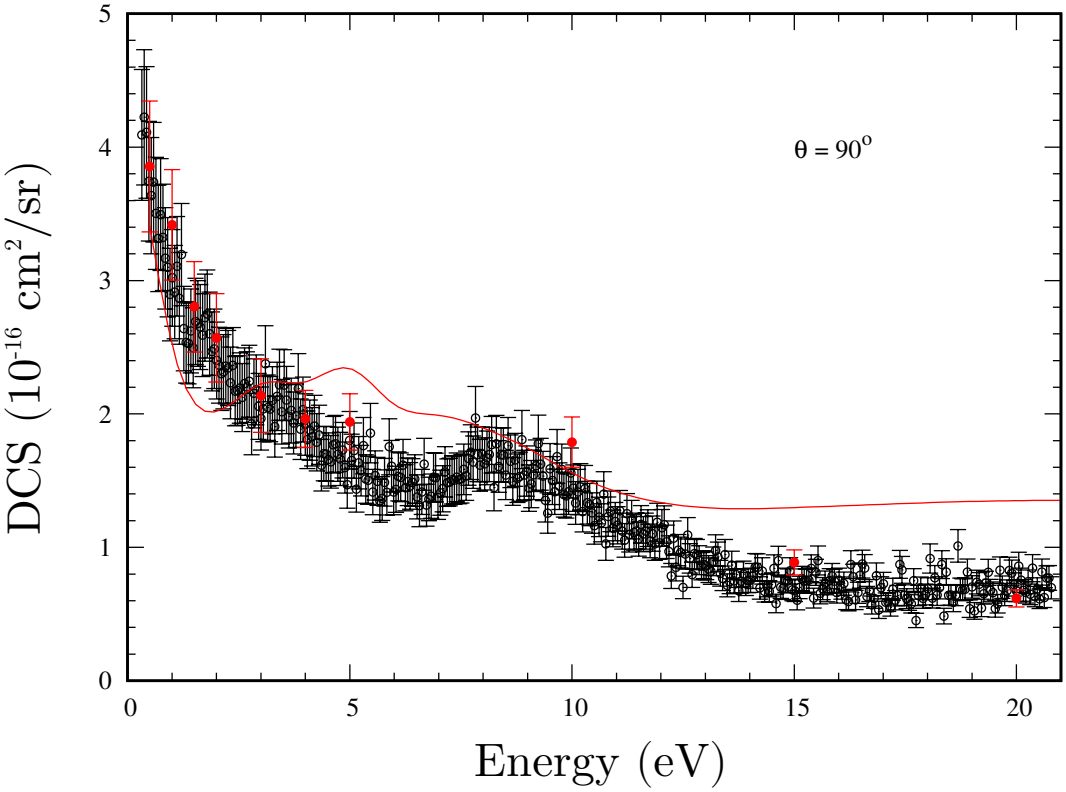

Figure 4. (color online) DCS for elastic scattering from CH_2Cl_2 at $\theta = 90^o$. (●) CSUF DCS from Table 1; (○) CSUF energy scan; (——) Present MCOP theory.

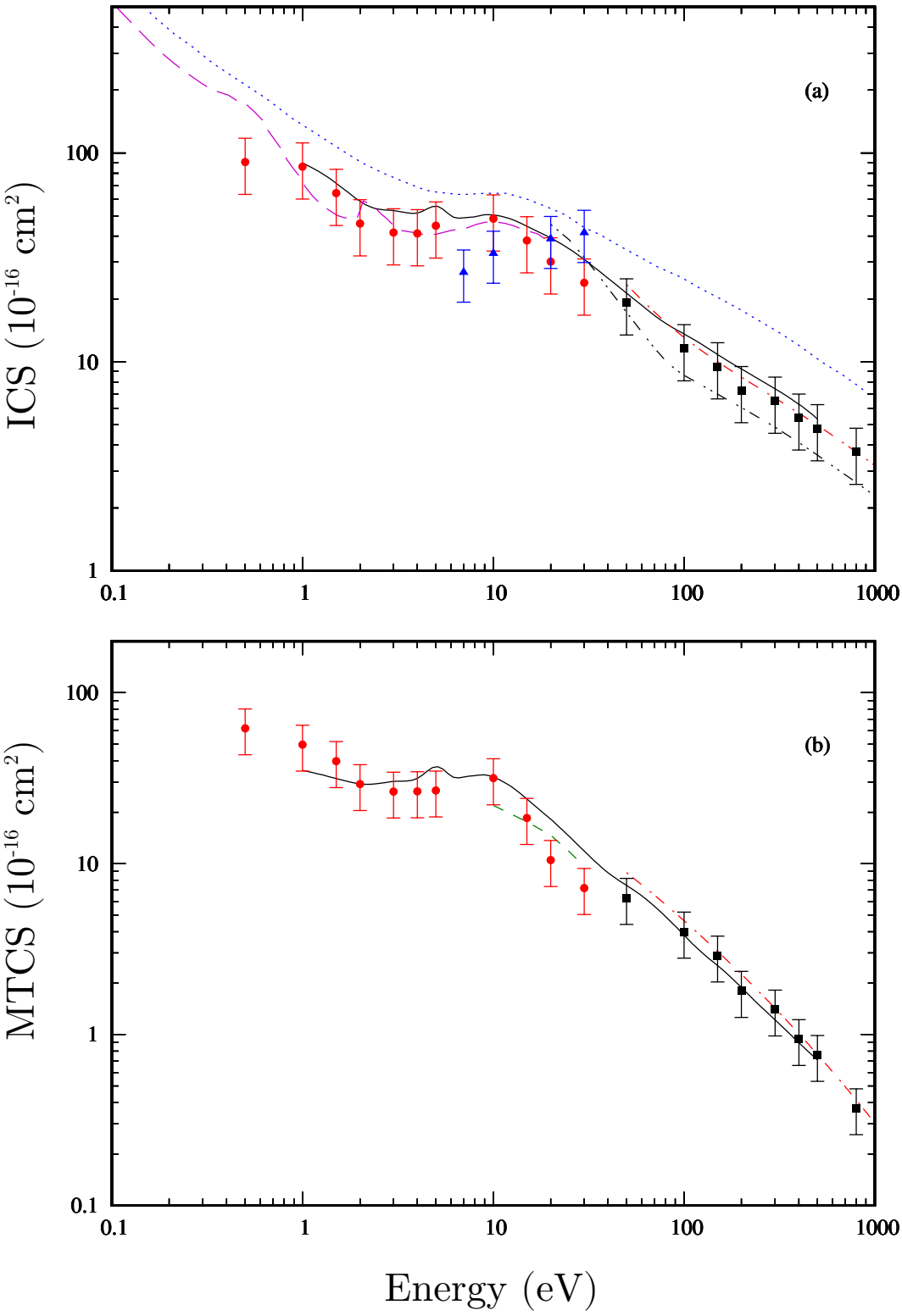

Figure 5. (color online) ICS and MTCS for elastic electron scattering from CH_2Cl_2. Legend: (●) Experiment, CSUF; (■) Experiment, UFSCar; (▲) Experiment [24]; (——) Present MCOP results; (-·-·-) Present IAM-AR results; (– – –) SMCPP + Born [24]; (·····) IAM-SCAR+I+Rot ICS results of [24]; (-·-·-) ICS results of Naghma *et al.* [23]; (- - -) SMC MTCS results of Natalense *et al.* [21]; see text for discussion.

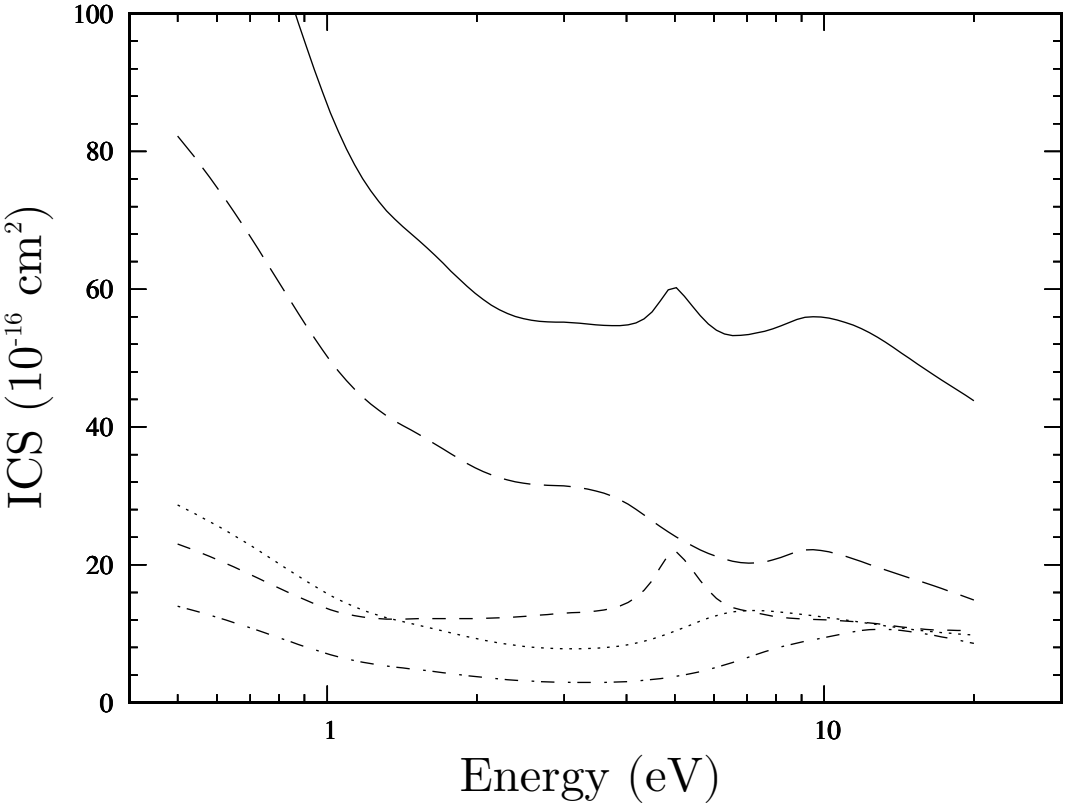

Figure 6. Partial-channel ICS for elastic electron scattering from CH_2Cl_2 calculated without Born-closure corrections. (———), A_1 channel; (– · – · –), A_2 channel; (·····), B_1 channel; (– – –), B_2 channel; (——), Summed ICS.

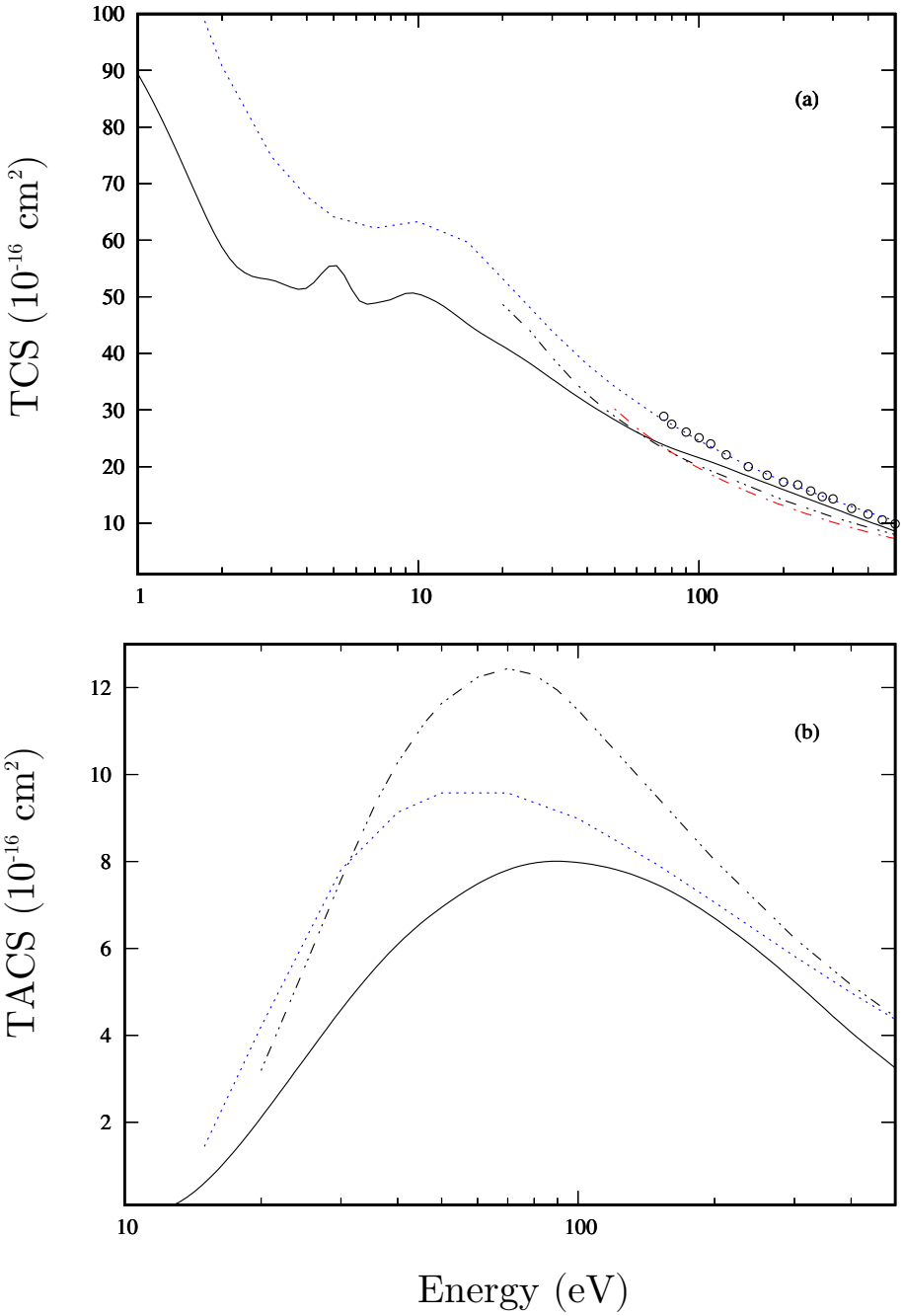

Figure 7. (a) TCS and (b) TACS for elastic electron scattering from CH_2Cl_2. In (a), the legend is same as Fig. 5, except (○), experimental TCS of Karwasz *et al.* [13].

Table 1. Experimental DCS (in 10^{-16} cm^2/sr), ICS and MTCS (in 10^{-16} cm^2) from the CSUF experiment for elastic electron scattering from CH_2Cl_2. The DCS estimated standard deviations are 20%. The estimated standard deviations of the ICS and MTCS are around 30%.

Angle	E(eV)										
(deg)	0.5	1.0	1.5	2.0	3.0	4.0	5.0	10.0	15.0	20.0	30.0
10	–	–	–	–	–	–	–	34.39	34.72	43.75	45.23
15	–	–	–	15.17	13.76	11.96	20.16	25.74	26.42	26.55	24.80
20	–	–	–	10.54	10.69	11.04	13.45	18.86	19.79	16.11	11.42
25	–	21.29	13.40	8.32	8.26	9.09	9.63	13.95	12.75	9.19	6.81
30	11.18	12.95	8.19	5.72	6.47	6.76	7.83	8.55	8.15	5.53	3.23
35	9.04	–	–	–	–	–	–	–	–	–	–
40	7.70	7.12	4.84	4.34	4.02	4.11	5.08	3.88	3.66	2.74	2.02
50	6.70	5.18	3.55	3.05	3.12	3.37	3.54	2.57	2.61	2.25	1.11
60	5.20	4.06	3.02	2.84	2.47	2.70	2.68	2.41	2.03	1.31	0.561
70	4.20	4.12	2.99	2.90	2.29	2.50	2.37	2.21	1.40	0.709	0.304
80	3.84	3.68	2.89	2.67	2.19	1.96	2.10	2.06	0.97	0.542	0.471
90	3.86	3.42	2.80	2.57	2.14	1.96	1.94	1.79	0.89	0.617	0.654
100	3.74	3.61	3.18	1.92	1.60	1.92	1.72	1.72	0.97	0.757	0.769
110	4.09	3.48	3.11	1.88	1.96	2.08	1.69	1.63	0.97	0.705	0.584
120	4.63	3.57	3.50	2.01	1.78	1.72	1.69	1.80	0.98	0.646	0.466
130	5.10	3.86	4.39	2.20	2.20	1.86	1.81	1.88	1.15	0.589	0.278
ICS	90.5	85.9	64.2	45.9	41.6	41.2	44.8	48.5	38.1	30.2	23.9
MTCS	61.9	49.7	39.8	29.2	26.4	26.5	26.8	31.6	18.5	10.5	7.2

Table 2. Experimental DCS (in 10^{-16} cm^2/sr), ICS and MTCS (in 10^{-16} cm^2) from the UFSCar experiment for elastic electron scattering from CH_2Cl_2. The DCS estimated standard deviations are 17% at 20 eV, 30 eV and 800 eV, 21% at 50 eV, and 11% at other energies See text for discussion. The estimated standard deviations of the ICS and MTCS are around 30%.

Angle	E(eV)									
(deg)	20	30	50	100	150	200	300	400	500	800
10	–	–	–	15.05	15.39	10.32	10.83	7.70	11.89	7.91
15	23.57	34.41	28.23	8.26	4.69	3.61	4.85	4.44	4.82	3.54
20	15.23	16.13	10.20	3.52	2.51	2.73	1.53	1.61	2.05	1.62
25	8.61	7.43	4.12	2.21	1.50	1.38	0.975	0.762	1.07	0.679
30	5.15	4.03	2.43	1.79	1.09	0.961	0.748	0.525	0.603	0.358
35	4.04	2.67	1.69	0.987	0.705	0.535	0.486	0.331	0.425	0.208
40	3.43	2.20	1.23	0.657	0.492	0.404	0.335	0.304	0.302	0.136
50	1.98	1.25	0.596	0.351	0.334	0.230	0.230	0.182	0.141	0.061
60	1.14	0.740	0.284	0.212	0.228	0.189	0.136	0.099	0.085	0.039
70	0.809	0.454	0.236	0.188	0.214	0.120	0.076	0.065	0.053	0.027
80	0.798	0.482	0.354	0.205	0.161	0.095	0.061	0.051	0.039	0.021
90	0.881	0.609	0.435	0.188	0.120	0.059	0.044	0.035	0.032	0.019
100	0.739	0.672	0.431	0.134	0.073	0.033	0.042	0.033	0.030	0.017
110	–	0.555	0.330	0.081	0.046	0.030	0.046	0.040	0.031	0.017
120	–	0.382	0.244	0.060	0.078	0.053	0.068	0.045	0.038	0.018
130	–	–	–	0.150	0.183	0.097	0.113	0.068	0.044	0.020
ICS	30.2	23.9	19.2	11.6	9.5	7.3	6.5	5.4	4.8	3.7
MTCS	10.5	7.2	6.3	4.0	2.9	1.8	1.4	0.94	0.76	0.37